Theoretical calculations of the contributions of excitation autoionization to electron-impact ionization in ions of the transition series of elements

D. C. Griffin* and C. Bottcher
Physics Division, Oak Ridge National Laboratory, Oak Ridge, Tennessee 37830

M. S. Pindzola
Department of Physics, Auburn University, Auburn, Alabama 36849

(Received 30 July 1981)

Electron-impact excitation of inner-shell electrons followed by autoionization can dominate the total ionization cross sections in certain cases. We have made calculations to investigate this phenomenon for transitions of the form $np^6nd^m \rightarrow np^5nd^{m+1}$ in ions of the transition series of elements. We predict such excitations lead to enhancements of the total cross section of more than an order of magnitude in the triply ionized species of Ti, Zr, and Hf in accord with recent crossed-beam experiments. In these cases, the predicted and measured positions and shapes of the resonances agree quite well; however, the magnitude of the theoretical cross sections is overestimated in the distorted-wave, dipole approximation used here. The effects of other kinds of excitation-autoionization transitions are considered, and trends along the first transition series are discussed.

I. INTRODUCTION

Excitation of inner-shell electrons to quasibound states, followed by autoionization can, in some cases, dominate the electron-impact ionization of positive ions. This was first demonstrated experimentally by Peart and Dolder[1] in 1975 for Ca^+, Sr^+, and Ba^+. In the case of Ba^+ the excitation-autoionization contribution to the cross section appears to be four times as large as the contribution from the direct process. In a recent letter,[2] experimental and theoretical results were presented which demonstrated that enhancements of more than an order of magnitude due, primarily, to excitations of the form

$$np^6nd^m \rightarrow np^5nd^{m+1}$$

can occur in the ionization cross sections of ions in the transition series of elements. It is apparent that such large effects must be included in equilibrium models for laboratory and astrophysical plasmas.

In this paper we consider details of, and extensions on, the theoretical aspects of the subject introduced in Ref. 2. In particular, we present the results of calculations of the positions and magnitudes of excitation-autoionization resonances due to the excitations

$$np^6nd \rightarrow np^5nd^2$$

in the triply ionized series elements Ti, Zr, and Hf. These results are compared to recent ionization cross-section measurements for these ions obtained from crossed-electron and ion beams.[2,3] In addition, we extend our discussion to other ions of the transition series of elements by considering the positions of $3p^53d^{m+1}$ configurations relative to the ionization thresholds in the elements ^{22}Ti through ^{31}Ga.

II. CALCULATIONAL METHODS

We assume that excitation-autoionization and direct ionization are independent processes so that the total ionization cross section, σ_{total}, is given by

$$\sigma_{\text{total}} = \sigma_{\text{direct}} + \sum_j \sigma^j_{\text{excit}} B^a_j \,, \tag{1}$$

where σ_{direct} is the direct ionization cross section, σ^j_{excit} is the excitation cross section of an inner-shell electron to an autoinizing level j, and B^a_j is the branching ratio for autoionization from the level j, which is given by

$$B^a_j = \frac{\sum_m A^a_{jm}}{\sum_m A^a_{jm} + \sum_k A^r_{jk}} \,, \tag{2}$$

where A^a_{jm} is the autoionization rate to channel m and A^r_{jk} is the radiative rate to a lower bound state k. The Lotz equation[4] was used to estimate the direct ionization cross section in all of our calculations because, in most cases,[5] it has been found to provide an upper limit to the contribution of the direct process.

In the distorted-wave approximation, the electron-impact excitation cross section for a transition of the form

$$k_i l_i + \alpha_i J_i \rightarrow k_f l_f + \alpha_f J_f$$

in an N-electron atom with total angular momenta J_i and J_f of the initial and final bound states is given by[6]

$$\sigma_{\text{excit}} = \frac{\pi a_0^2}{k_i^2 2(2J_i+1)} \sum_{\substack{l_i l_f \\ J_i J_f \mathcal{J}}} (2\mathcal{J}+1) \, | \, T(\alpha_i J_i, l_i J_i \mathcal{J}; \alpha_f J_f, l_f j_f \mathcal{J}) \, |^2 \tag{3}$$

where α_i and α_f are used to represent all other quantum numbers needed to specify the initial and final bound states in an arbitrary coupling scheme; k_i, l_i, and j_i are the wave number, orbital angular momentum, and total angular momentum, respectively, of the incident electron; k_f, l_f, and j_f are the wave number, orbital angular momentum, and total angular momentum, respectively, of the scattered electron; $\mathcal{J}$ is the total angular momentum of the $N+1$ electron system; and $T(\alpha_i J_i, l_i j_i \mathcal{J}; \alpha_f J_f, l_f j_f \mathcal{J})$ is an element of the transition matrix $\underline{T}$. The transition matrix is in turn related to the reactance matrix $\underline{R}$, by the equation $\underline{T} \cong -2i\underline{R}$, in the weak-coupling limit that the elements of $\underline{R}$ are $<<1$, where

$$R(\alpha_i J_i, l_i j_i \mathcal{J}; \alpha_f J_f, l_f j_f \mathcal{J}) \cong -\langle \Psi(\alpha_i J_i, (l_i, \tfrac{1}{2}) j_i \mathcal{J}) \left| \sum_{j=1}^{N} \frac{2}{r_{j,N+1}} \right| \Psi(\alpha_f J_f (l_f, \tfrac{1}{2}) j_f \mathcal{J}) \rangle \tag{4}$$

and $\Psi(\alpha J, (l, \frac{1}{2}) j \mathcal{J})$ is an antisymmetrized, coupled, $N+1$ electron wave function. The final coupling between the bound state (characterized by the total angular momentum J) and the orbital and spin angular momenta of the continuum electron is performed in a $J-j$ fashion. In Eq. (4), we have assumed that the radial part of the one-electron continuum wave functions are normalized to a value of $1/\sqrt{k}$ as $r \rightarrow \infty$, that the spin orbitals for the initial and final states of the active electron are orthogonal, and that the overlap between the continuum wave functions and the bound-state spin orbitals are negligible.

The calculation of the elements of $\underline{R}$ is quite complicated for transitions of the type $np^6 nd^m \rightarrow np^5 nd^{m+1}$. Therefore, since the primary purpose of this work is to predict where large indirect enhancements of the total cross section may occur and to estimate their magnitude, we have neglected configuration-interaction effects within the target ion, assumed that the elements of the reactance matrix are small, and retained only in the direct-dipole term in calculating the reactance matrix, from Eq. (4). We present a derivation of the expression for the excitation cross section in this approximation in the Appendix.

For the results reported here, the radial wave functions of the bound-state spin orbitals were calculated using the Hartree-Fock method with relativistic modifications (HFR),[7] and the continuum wave functions were computed using a semiclassical exchange potential.[8] The continuum wave function for both the incident and scattered electrons were calculated in the potential of the final (autoionizing) state. All angular momenta of the incident electron up to 10 were included in the present calculation, the contribution from higher values having been found negligible.

The energy levels and branching ratios were determined using an atomic-structure program provided by Cowan.[9] The average energies of configurations, electrostatic parameters, and spin-orbit parameters were calculated with HFR radial wave functions. Following standard procedures, the energy levels within a configuration were corrected for the effects of correlation by scaling the HFR electrostatic parameters. For these calculations, a scaling factor of 0.80 was selected, since it provided good agreement between experimental and calculated energies for the bound-state levels of $3p^5 3d^2$ in V^{4+}.[10]

III. RESULTS AND DISCUSSION

Results of our calculations of the positions of the $np^5 nd^2$ configurations relative to the ionization

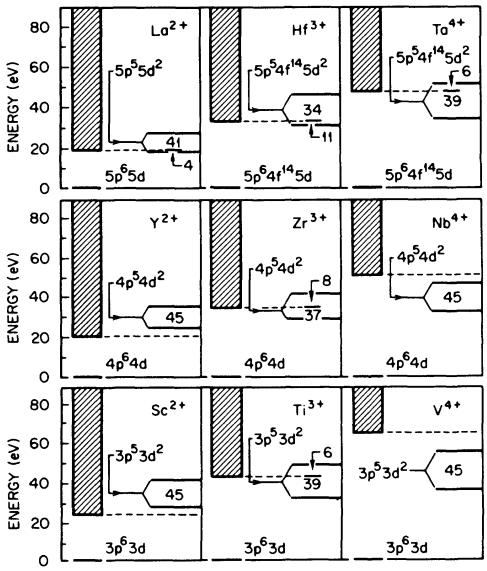

FIG. 1. Energy-level structure of np^5nd^2 relative to the ionization threshold for several ions of the transition series of elements. The shaded areas indicate the continuum, and the number of levels above and below the respective ionization thresholds is indicated for each case.

thresholds in $+2$, $+3$, and $+4$ ions of the transition-series elements are shown in Fig. 1. As the charge state increases, the ionization potentials increase more rapidly than the energies of the levels of p^5d^2 so that they become bound and cannot autoionize. As can be seen, the p^5d^2 configuration in Ti^{3+}, Zr^{3+}, and Hf^{3+} lie on the edge with levels both above and below the ionization threshold. However, in all three cases, levels above the ionization thresholds contain most of the oscillator strength of the $np \rightarrow nd$ transitions. For this reason, we would expect these ions to exhibit large contributions from excitation autoionization in the ionization cross sections near threshold.

Details for the energy levels of the $3p^53d^2$ configuration in Ti^{3+} are shown in Fig. 2. There are six levels and three terms, labeled by their LS designations, above the ionization threshold. The

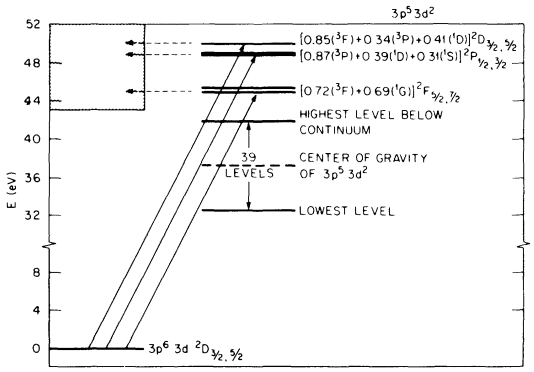

FIG. 2. Details of the energy-level diagram of $3p^53d^2$ in Ti^{3+} relative to the ionization limit. The designations of the autoionizing levels are given in LS notation.

various parents of the three doublet terms are strongly mixed due to large off-diagonal electrostatic elements. The average energies, branching ratios, oscillator strengths, and distorted-wave dipole excitation cross sections at threshold are given for these three terms in Table I. The only branching ratio that differs appreciably from 1 is that associated with the ^2D term. If this term was pure, it could not autoionize the continuum states of $3p^6kl$ and still conserve parity. However, it can radiate to the ground-state term $3p^63d^2D$. Therefore, this branching ratio is nonzero only because of a small amount of mixing with the ^2P and ^2F terms.

A comparison of the experimental and theoretical results for the ionization cross section in the energy region near the ionization limit is shown in Fig. 3. The data reveal a very large departure from the Lotz formula in which two prominent structures appear at approximately 44.5 and 47.5 eV. These are identified with the three terms listed in Table I, with the last two terms being unresolved experimentally. However, a scaling factor of 0.4 is required to bring the Lotz-plus-distorted-wave dipole calculations of the total ionization cross section into agreement with experiment. In order to determine the approximate magnitude of

TABLE I. Autoionizing terms of Ti^{3+} $3p^53d^2$.

LS designation	Energy (eV)	B^a	f	σ (10^{-18} cm^2)
$[0.72(^3F)+0.69(^1G)]^2F$	44.5	1.000	1.627	36.6
$[0.87(^3P)+0.39(^1D)+0.31(^1S)]^2P$	48.0	0.996	1.056	21.8
$[0.85(^3F)+0.34(^3P)+0.41(^1D)]^2D$	49.1	0.416	2.180	43.9

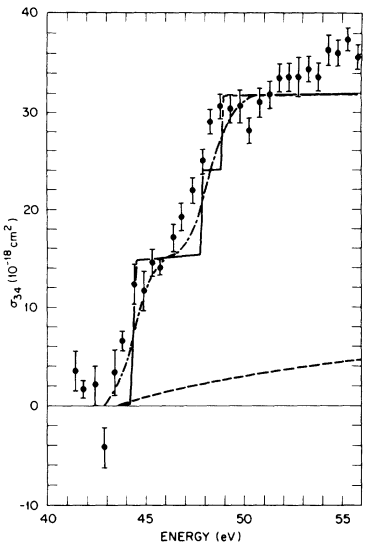

FIG. 3. Electron-impact ionization cross section for Ti^{3+}. Dashed curve is an estimate of the direct ionization cross section from the semiempirical formula of Lotz (Ref. 4). Solid line is Lotz-plus-distorted-wave dipole multiplied by 0.40. Dot-dashed curve is the solid line convoluted with a 2-eV FWHM Gaussian, chosen to simulate the electron energy spread. Experimental points are from Falk *et al.* (Refs. 2 and 3).

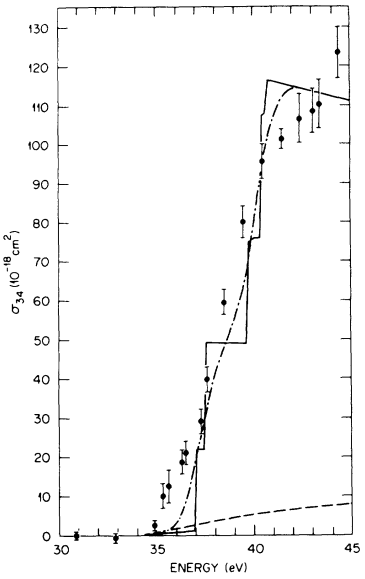

FIG. 4. Electron-impact ionization cross section for Zr^{3+}. The notation is the same as for Fig. 3.

the error made by neglecting exchange, we calculated the excitation cross section to the ^2F term at 44.5 eV including the exchange terms. We obtained a value of 28.6×10^{-18} cm^2 for the cross section at threshold, as compared with the dipole value of 36.6×10^{-18} cm^2. This 22% reduction in the cross section improves agreement with experiment, but it is still nearly twice as large as the experimental result at this energy. Unitarizing the reactance matrix would provide additional improvement; however, the effects of configuration interaction are also important. For example, mixing between the ground-state configuration $3p^6 3d$ and $3p^4 3d^3$ is found to reduce the oscillator strength to $3p^5 3d^2$ by about 20%. Additional interactions with the $3p^5 3d^2$ configuration may also be significant.

When our Lotz-plus-distorted-wave dipole calculations are scaled by 0.40 and convoluted with a 2-eV FWHM Gaussian to simulate the experimental energy spread, the agreement with the experimental results is quite good. This confirms our identification of the resonance and indicates that the agreement between the theoretical and experimental results for the threshold energies is well within the experimental and theoretical uncertainties. We believe that the additional rise in the experimental cross section, which begins at approximately 52 eV, is due to excitation-autoionization effects within other configurations. It is the contribution of these other configurations (which we have not included) that makes it impossible to compare meaningfully our results with experiment at higher energies, where our approximations are more valid.

Similar comparisons between experiment and theory for Zr^{3+} and Hf^{3+} are shown in Figs. 4 and 5. In the case of Zr^{3+}, the total cross-section calculations, when scaled by the same factor of 0.40 and convoluted, also fit the data quite well although the levels are here too close together to be resolved experimentally. The comparison between the calculated and experimental cross sections for Hf^{3+} is much less satisfactory. Not only is the predicted magnitude too large, but the shape of the theoretical cross section near threshold differs considerably from the experimental data. In fact, the scaled convoluted cross section falls below experiment between 33 and 45 eV. A possible explanation for this discrepancy may be found by referring to Fig. 1. We see that 34 levels of the $5p^5 4f^{14} 5d^2$ configuration lie above the ionization threshold in Hf^{3+}. Transitions to all but 11 of these levels are very weak in the dipole approximation, and they can be reached from the gound state only through higher-order multipoles and exchange. Therefore, transitions to these levels are not included in our calculations; but since the levels mostly lie in the

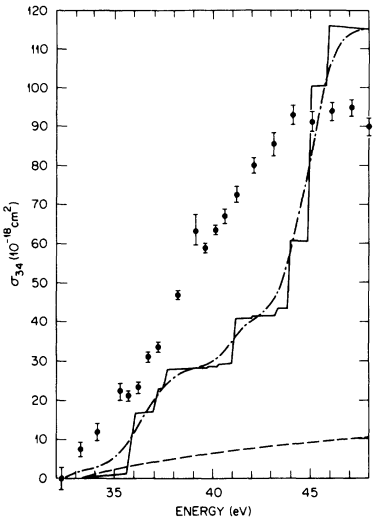

FIG. 5. Electron-impact ionization cross section for Hf^{3+}. The notation is the same as for Fig. 3.

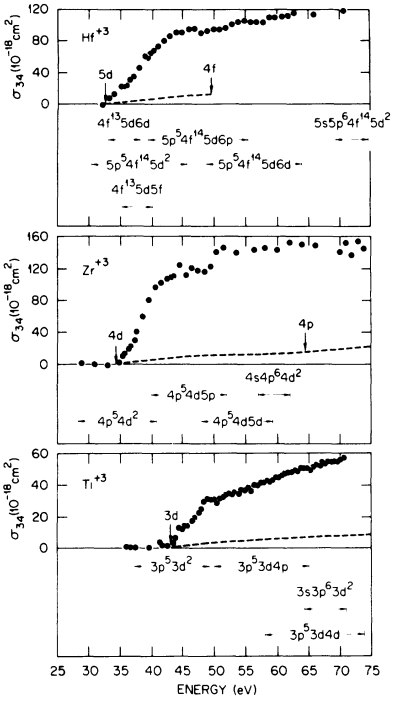

FIG. 6. Experimental electron-impact ionization cross sections for Ti^{3+}, Zr^{3+}, and Hf^{3+} over the energy range for which autoionizing resonances appear to occur; data from Falk *et al.* (Refs. 2 and 3). The dots are the experimental points and the dashed curve is the direct ionization cross section calculated from the semiempirical formula of Lotz. Positions of configurations believed to contribute to autoionization are shown below each curve.

above-mentioned energy range, such dipole-forbidden transitions may account for the discrepancy in shape.

Figure 6 shows the experimental cross sections for all three ions over the energy ranges where the indirect process appears to add to the total ionization cross sections. Using Lotz as an upper limit on the cross section for direct ionization, it is apparent that the indirect enhancement is at least a factor of 10 for Ti^{3+} and Hf^{3+}, and 20 for Zr^{3+}. Furthermore, these data reveal that quasibound levels from other configurations must be involved, since the cross sections continue to rise at energies above the highest level of np^5nd^2. The positions of various configurations which may contribute to the total cross sections are shown below each set of data. In addition to np^5nd^2, for Ti^{3+} and Zr^{3+} we have three configurations formed from the inner-shell excitations $np \rightarrow (n+1)p$, $np \rightarrow (n+1)d$, and $ns \rightarrow nd$ which appear to provide an appreciable contribution to the total cross section. For example, in the case of Ti^{3+} the experimental cross section increases by approximately 25×10^{-18} cm^2 from 49 to 75 eV, while the Lotz equation predicts an increase of only 5×10^{-18} cm^2 due to the direct process; in addition, the contribution due to the $3p^53d^2$ configuration should fall off over this energy range, making this rise in the cross section even more significant. In the case of Hf^{3+}, in addition to the configurations mentioned above, there are two configurations formed by the inner-shell excitations $4f \rightarrow 6d$ and $4f \rightarrow 5f$. Since these configurations overlap the $5p^54f^{14}5d^2$ configuration, they may also contribute to the discrepancy between the scaled, convoluted theory and the experimental results shown in Fig. 5. The implication of these results is in that excitations other than $\Delta n = 0$, dipole transitions can make significant excitation-autoionization contributions to the total electron impact ionization cross sections in complex ions. This further complicates attempts to make accurate theoretical predictions of the effects of excitation-autoionization in complex species.

In an effort to determine the importance of $np^6nd^m \rightarrow np^5nd^{m+1}$ excitation-autoionization transitions in other ions of the transition-series elements, we have calculated the positions of np^5nd^{m+1} configurations for the threefold and fourfold ions of elements within the first transition series relative to their ionization thresholds. Figure 7 shows the results of these calculations for the triply ionized species of Ti^{3+} (the first + 3 ion for which levels of $3p^53d^{m+1}$ are autoionizing) through Fe^{3+}, where all but 3 of the 200 levels of

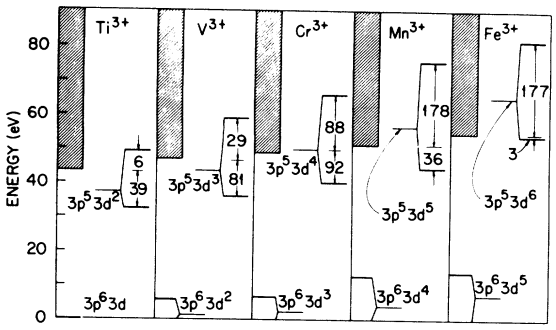

FIG. 7. Energy-level diagrams of $3p^5 3d^{m+1}$ configurations in threefold ionized atoms of the first transition series relative to their ionization thresholds. The number of levels above and below the ionization limit is shown in each case.

$3p^5 3d^6$ are autoionizing. As the atomic number increases, the levels of $3p^5 3d^{m+1}$ rise in energy more rapidly than the ionization thresholds; therefore, more and more levels of $3p^5 3d^{m+1}$ become autoionizing as we move across the transition series. From Co^{3+} to Zn^{3+} (where $m+1=10$) all levels of $3p^5 3d^{m+1}$ are above the ionization thresholds. Results for the fourfold-ionized elements, Mn^{4+} (the first $+4$ ion for which levels of $3p^5 3d^{m+1}$ are autoionizing) through Ga^{4+}, are shown in Fig. 8. The trend as a function of Z is the same as for the $+3$ results. Our calculations indicate that the levels of $3p^5 3d^{m+1}$ are all bound for ionization stages of $+5$ or greater. One might conclude from this that large effects due to excitation-autoionization should disappear in these higher stages of ionization; however, the results for Ti^{3+}, Zr^{3+}, and Hf^{3+} indicate that excitations other than these $\Delta n=0$ dipole transitions can also make appreciable contributions to the total ionization cross sections. In addition, other studies[11,12] have shown that the relative importance of $\Delta n>0$, dipole excitation-autoionizing transitions tends to increase as a function of ionization stage.

A summary of those ions within the first transition series for which $3p^6 3d^m \rightarrow 3p^5 3d^{m+1}$ transitions are autoionizing is given in Table II. Similar results are expected for the second and third transition series beginning with Y^{2+} and La^{2+} respectively. However, it would be misleading to assume that all of these ions show autoionizing effects due to these transitions that are as large as those that have been observed in Ti^{3+}, Zr^{3+}, and Hf^{3+}. Our dipole calculations indicate that the $3p \rightarrow 3d$ excitation cross sections will have a general tendency to decrease as we move along a particular transition series, filling the outer d subshell. At the same time, the direct ionization cross sections become larger as the number of d electrons increases. Therefore, the ratio of the cross sections for indirect-to-direct ionization is smaller in an ion such as Fe^{3+} than it is in Ti^{3+}. The result of our cross-section calculation for transitions from the ground-state ^6S term in Fe^{3+} is shown in Fig. 9. The dipole-plus Lotz results indicate an indirect enhancement of approximately 2.5. This calculation surely overestimates the excitation cross sections for the dipole-allowed transitions; however, it does not include the contributions of dipole-forbidden transitions of $3p^5 3d^6$ or transitions to other autoionizing configurations, which will add to the total indirect enhancement. Thus, since these errors will tend to cancel, our calculations should provide a factor-of-2 estimate of the indirect enhancement in such complex ions.

There is an important difference concerning these effects in $+3$ and $+4$ ions. In the $+3$ ions, all those levels that have strong dipole transi-

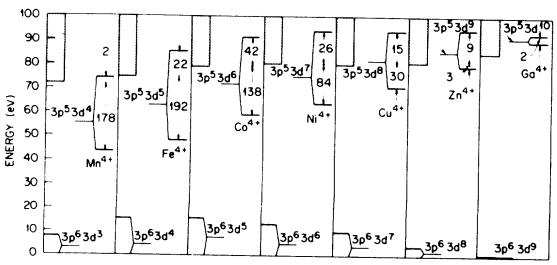

FIG. 8. Energy-level diagrams of $3p^5 3d^{m+1}$ configurations in fourfold ionized atoms of the first transition series relative to the ionization thresholds. The number of levels above and below the ionization limit is shown in each case.

TABLE II. Autoionizing transitions in ions of the transition series.

Transition	Ions
$3p^6 3d \rightarrow 3p^5 3d^2$	Sc^{2+}, Ti^{3+}
$3p^6 3d^2 \rightarrow 3p^5 3d^3$	Ti^{2+}, V^{3+}
$3p^6 3d^3 \rightarrow 3p^5 3d^4$	V^{2+}, Cr^{3+}, Mn^{4+}
$3p^6 3d^4 \rightarrow 3p^5 3d^5$	Cr^{2+}, Mn^{3+}, Fe^{4+}
$3p^6 3d^5 \rightarrow 3p^5 3d^6$	Mn^{2+}, Fe^{3+}, Co^{4+}
$3p^6 3d^6 \rightarrow 3p^5 3d^7$	Fe^{2+}, Co^{3+}, Ni^{4+}
$3p^6 3d^7 \rightarrow 3p^5 3d^8$	Co^{2+}, Ni^{3+}, Cu^{4+}
$3p^6 3d^8 \rightarrow 3p^5 3d^9$	Ni^{2+}, Cu^{3+}, Zn^{4+}
$3d^6 3d^9 \rightarrow 3p^5 3d^{10}$	Cu^{2+}, Zn^{3+}, Ga^{4+}

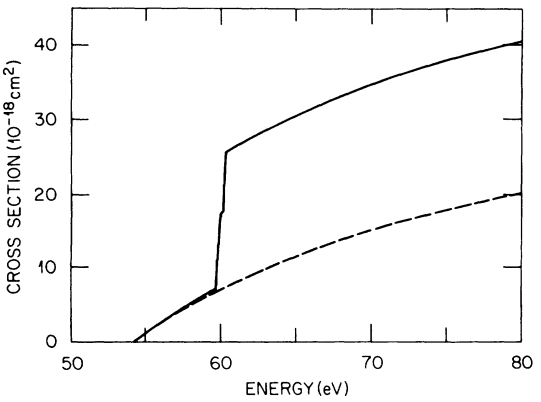

FIG. 9. Electron-impact ionization cross section for Fe^{3+}. Notation is similar to Fig. 3.

tions from the levels of the ground-state term are autoionizing. Thus, as the number of autoionizing levels increases with atomic number, the additional contributions to the cross section should be relatively small. However, in the $+4$ ions of Mn, Fe, Co, and Ni, those levels of $3p^5 3d^{m+1}$ which show strong dipole transitions from the levels of the lowest term of $3p^6 3d^m$ are bound. There are strong dipole transitions to autoionizing levels of $3p^5 3d^{m+1}$ from the higher-energy metastable levels of the ground-state configuration. Thus, the magnitude of the autoionizing effects in these ions, being dependent entirely on how the metastable levels are populated, will be sensitive to the effective temperature of the ion source. This phenomenon is illustrated in Fig. 10 for the case of Fe^{4+}. For an

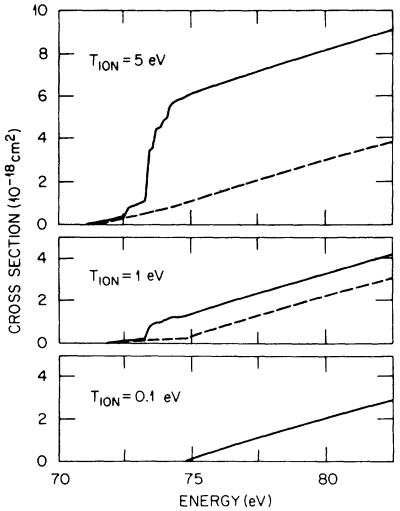

FIG. 10. Electron-impact ionization cross section for Fe^{4+}, showing the sensitivity of the indirect process to the temperature of the source. The notation is similar to Fig. 3.

ion temperature of 0.1 eV only the lowest term $3p^6 3d^4\,{}^5D$ is populated, and (in our dipole approximation) the indirect contribution is negligible. However, at a temperature of 1 eV some of the higher-energy terms of $3p^6 3d^4$ are populated, and the indirect ionization cross section is measurable. As the temperature is increased to 5 eV, the indirect contribution increases significantly but for temperatures above 5 eV does not show any additional changes. The source temperature also affects the effective ionization energy and the direct ionization cross section, as can be seen in Fig. 10. Our conclusion may be modified when nondipole transitions are properly included. Nonetheless since the dominant dipole transitions are only possible at higher temperatures, the cross sections will still tend to increase with temperature. In the cases of Cu^{4+}, Zn^{4+}, and Ga^{4+}, the levels of the upper configuration that show strong dipole transitions from the lowest levels of the ground-state configuration are autoionizing, and this extreme temperature sensitivity of the indirect enhancement disappears.

In conclusion, autoionizing effects should be important in many ions of the transition-series elements, although accurate calculations of the magnitude of the contributions to the total ionization cross sections are very difficult because of the complexity of the configurations involved. The dipole approximation may provide a reasonable method of estimating these effects and could be included in the calculation of ionization rates for ions such as Fe^{2+}, Fe^{3+}, and Fe^{4+}, which are important in fusion-related plasmas near the walls of the containment vessel.

ACKNOWLEDGMENTS

The authors are indebted to R. D. Cowan for making his atomic-structure program available to us and for many helpful discussions. We also wish to acknowledge J. B. Mann and S. M. Younger for a number of useful conversations, and R. A. Falk, G. H. Dunn, D. C. Gregory, and D. H. Crandall for providing us with their complete data before publication. Finally, the first author is pleased to acknowledge the Great Lakes Colleges Association and the Associated Colleges of the Midwest for their support of his professional leave at the Oak Ridge National Laboratory. This work was supported through the Office of Fusion Energy, U. S. Department of Energy under contract W-7405-ENG-26 with the Union Carbide Corporation.

APPENDIX

We consider the dipole approximation to the excitation cross section for cases in which the initial and final bound states are calculated in a single-configuration approximation. First we employ the well-known expansion

$$\frac{2}{r_{j,N+1}}=\sum_{\lambda}\frac{2r_<^{\lambda}}{r_>^{\lambda+1}}P_{\lambda}(\vec{r}_j\cdot\vec{r}_{N+1})=\sum_{\lambda}\frac{2r_<^{\lambda}}{r_>^{\lambda+1}}C_{(j)}^{(\lambda)}\cdot C_{(N+1)}^{(\lambda)}\ , \tag{A1}$$

where $C_{(j)}^{(\lambda)}\cdot C_{(N+1)}^{(\lambda)}$ is the scalar product of tensors of order λ, the components of which are defined by the equation

$$C_q^{(\lambda)}=\left[\frac{4\pi}{2\lambda+1}\right]^{1/2}Y_{\lambda q} \tag{A2}$$

and $Y_{\lambda q}$ is the spherical harmonic. Using Eq. (A1) in Eq. (4), and representing $R(\alpha_i J_i,l_i J_i \mathscr{J};\alpha_f J_f,l_f J_f \mathscr{J})$ by $R(i;f)$ we obtain

$$R(i;f)=-\sum_{\lambda}\left\langle\Psi(\alpha_i J_i,(l_i,\tfrac{1}{2})j_i\mathscr{J})\left|\sum_{j=1}^{N}\frac{2r_<^{\lambda}}{r_>^{\lambda+1}}C_{(j)}^{(\lambda)}\cdot C_{(N+1)}^{(\lambda)}\right|\Psi(\alpha_f J_f,(l_f,\tfrac{1}{2})j_f\mathscr{J})\right\rangle\ . \tag{A3}$$

Now we neglect exchange and assume that Ψ is a coupled, simple-product wave function. In this case, we can employ Eq. (11.47) of Ref. 9

$$R(i;f)=(-1)^{J_f+j_i+\mathscr{J}+1}\sum_{\lambda}\begin{Bmatrix}J_i & j_i & \mathscr{J}\\ j_f & J_f & \lambda\end{Bmatrix}\langle\alpha_i J_i\left|\left|\sum_{j=1}^{N}C_{(j)}^{(\lambda)}\right|\right|\alpha_f J_f\rangle\langle(l_i,\tfrac{1}{2})j_i\left|\left|C_{(N+1)}^{(\lambda)}\right|\right|(l_f,\tfrac{1}{2})j_f\rangle R_d^{\lambda}\ , \tag{A4}$$

where the direct Slater integral R_d^{λ} is given by the equation

$$R_d^{\lambda}=\int_0^{\infty}\left[\frac{2}{r_2^{\lambda+1}}\int_0^{r_2}r_1^{\lambda}P_{nl}(r_1)P_{n'l'}(r_1)\,dr_1+r_2^{\lambda}\int_{r_2}^{\infty}\frac{2}{r_1^{\lambda+1}}P_{nl}(r_1)P_{n'l'}(r_1)\,dr_1\right]F_{k_i l_i}(r_2)F_{k_f l_f}(r_2)\,dr_2 \tag{A5}$$

and $P_{nl}(r)$ and $F_{kl}(r)$ are the radial parts of the bound state and continuum one-electron wave functions, respectively. Furthermore, using Eq. (11.38) of Ref. 9, we find that

$$\langle(l_i,\tfrac{1}{2})j_i\left|\left|C_{(N+1)}^{(\lambda)}\right|\right|(l_f,\tfrac{1}{2})j_f\rangle=(-1)^{l_i+1/2+j_f+\lambda}\sqrt{(2j_i+1)(2j_f+1)}\begin{Bmatrix}l_i & \frac{1}{2} & j_i\\ j_f & \lambda & l_f\end{Bmatrix}\langle l_i\left|\left|C^{(\lambda)}\right|\right|l_f\rangle\ . \tag{A6}$$

We now drop all terms other than $\lambda=1$ (dipole approximation), insert Eqs. (A4), (A6), and the expression for T given just above Eq. (4) into Eq. (3) and make use of the orthonormal relation for 6-j symbols[13] to obtain

$$\sigma_{\text{excit}}=\frac{4\pi a_0^2}{3k_i^2(2J_i+1)}\left|\langle\alpha_i J_i\left|\left|\sum_{j=1}^{N}C_{(j)}^{(1)}\right|\right|\alpha_f J_f\rangle\right|^2\sum_{l_i l_f}\left|\langle l_i||C^{(1)}||l_f\rangle\right|^2(R_d^1)^2\ . \tag{A7}$$

Introducing the optical oscillator strength $f_{J_i J_f}$ we find

$$\sigma_{\text{excit}}=\frac{4\pi a_0^2}{k_i^2}\frac{f_{J_i J_f}}{\Delta E}\sum_{l_i l_f}\frac{l_>[R_d^1(l_i,l_f)]^2}{[P_{nl}\mid r\mid P_{n'l'}]^2}\ , \tag{A8}$$

where $[P_{nl}\mid r\mid P_{n'l'}]$ is the radial dipole moment

$$[P_{nl}\mid r\mid P_{n'l'}]=\int_0^{\infty}P_{nl}(r)rP_{n'l'}(r)\,dr\ . \tag{A9}$$

It is instructive to relate our procedure to the well-known effective Gaunt equation[14,15]

$$\sigma_{\text{excit}}=\frac{8\pi}{\sqrt{3}}\frac{1}{k_i^2\Delta E}f_{J_i J_f}g\pi a_0^2\ , \tag{A10}$$

where g is then given by the equation

$$g=\frac{\sqrt{3}}{2\pi}\sum_{l_i l_f}\frac{l_>[R_d^1(l_i,l_f)]^2}{[P_{nl}\mid r\mid P_{n'l'}]^2}\ . \tag{A11}$$

It should be noted that this equation for g is different from the definition of the effective Gaunt factor in Ref. 15; the former was derived from the Bethe approximation. The advantage of Eq. (A8) is that is allows one to calculate the excitation cross section in the dipole approximation in terms of the oscillator strength, which in our case is calculated using the atomic structure program. The radial dipole moments are computed using HFR wave functions and R_d^1 is computed using HFR bound-state radial wave functions and the distorted-wave radial wave functions.

---

*On sabbatical leave from Rollins College, Winter Park, Florida.

[1]B. Peart and K. Dolder, J. Phys. B 1, 872 (1968); and 8, 56 (1975): also see work on Ba^+ by B. Peart, J. G. Stevenson, and K. Dolder, *ibid.* 6, 146 (1973); R. K. Feeney, J. W. Hooper, and M. T. Elford, Phys. Rev. A 6, 1469 (1972).

[2]R. A. Falk, G. H. Dunn, D. C. Griffin, C. Bottcher, D. C. Gregory, D. H. Crandall, and M. S. Pindzola, Phys. Rev. Lett. 47, 494 (1981).

[3]R. A. Falk, G. H. Dunn, D. C. Gregory, and D. H. Crandall (private communication).

[4]W. Lotz, Z. Phys. 220, 466 (1969); and Z. Phys. 216, 241 (1968).

[5]For example, see, D. H. Crandall, Phys. Scr. 23, 153 (1981).

[6]This reduces to the more familiar equation

$$\sigma_{\text{excit}} = \frac{\pi a_0^2}{k_i^2 2(2L_i+1)(2S_i+1)} \times \sum_{\substack{l_i,l_f \\ \mathscr{L},\mathscr{S}}} (2\mathscr{L}+1)(2\mathscr{S}+1) \times |T(\alpha_i L_i S_i, l_i \mathscr{L}\mathscr{S}; \alpha_f L_f S_f, l_f \mathscr{L}\mathscr{S})|^2 ,$$

when the spin-orbit interactions among the bound-state electrons are small and the total orbital and spin angular momenta of the bound states are good quantum numbers.

[7]R. D. Cowan and D. C. Griffin, J. Opt. Soc. Am. 66, 1010 (1976).

[8]M. E. Riley and D. G. Truhlar, J. Chem. Phys. 63, 2182 (1975).

[9]The atomic structure program is described by R. D. Cowan, in *The Theory of Atomic Structure and Spectra* (University of California Press, Berkeley, 1981).

[10]C. H. H. Van Deurzen, J. Opt. Soc. Am. 67, 476 (1977).

[11]D. H. Crandall, R. A. Phaneuf, B. E. Hasselquist, and D. C. Gregory, J. Phys. B 12, L249 (1979).

[12]R. D. Cowan and J. B. Mann, Astrophys. J. 232, 940 (1979).

[13]M. Rotenberg, R. Bivins, N. Metropolis, and J. K. Wooten, *The 3-j and 6-j Symbols* (Technology Press, Cambridge, Mass., 1959).

[14]M. J. Seaton, in *Atomic and Molecular Processes,* edited by D. R. Bates (Academic, New York, 1962), Chap. 11.

[15]H. van Regemorter, Astrophys. J. 136, 906 (1962).